Journal of Machine Engineering, 2022, Vol. 22, No. 2, No. 2, 68–79
ISSN 1895-7595 (Print) ISSN 2391-8071 (Online)

Received: *18 February 2022* / Accepted: *09 May 2022* / Published online: *16 May 2022*

compliant joints,
gantry stage, accuracy

Patrick PÖHLMANN[1*], Christoph PEUKERT[1],
Marcel MERX[1], Jens MÜLLER[1],
Steffen IHLENFELDT[1,2]

COMPLIANT JOINTS WITH REMOTE CENTRE OF COMPLIANCE FOR THE IMPROVEMENT OF THE MOTION ACCURACY OF A GANTRY STAGE

Gantry stages, which consist of two parallel acting servo drives, are commonly used in machine tools. One drawback of this concept is the crosstalk between both drives, when a stiff mechanical coupling is present. This can lead to a limited bandwidth of the position control or to high reaction forces. One way to overcome these issues is the usage of joints to create an additional degree of freedom, which allows the drives to move independently. The design of these joints as compliant elements offers advantages compared to common rolling bearings, such as low friction and the absence of backlash. Another benefit is the variability in the design of the compliant joints allowing for adjustments to the position of each joint's centre of compliance. Thus, the position of the resulting pivot, and the transfer matrix between the motion of the drives and the motion at the gantry stage's tool centre point, change as well. This paper addresses the placement of the joint's centre of compliance in order to improve motion accuracy. For this purpose, joints with modular arranged compliant links have been designed. The characteristics of the joints and their effect on the behaviour of the gantry stage are compared using analytical investigations as well as experimental results.

1. INTRODUCTION

High productivity and high accuracy are essential goals in the development of machine tools and production systems in general. The enhancement of a motion system's feed drive dynamics is one strategy to increase its productivity. Thus, higher drive forces are required and can lead to a reduction in accuracy if the machine structure is dynamically excited. A gantry-type motion system, which consists of two parallel acting drives, has the ability to reduce structural disturbances if drive forces are applied to the centre of gravity of the moved assembly [1]. However, using two drives for one degree of freedom (DOF) can lead to stability issues in the control loops of the drives due to their mechanical coupling [2]. In this case, the bandwidth of the motion control and thus the motion dynamics of the entire system

[1] Faculty of Mechanical Science and Engineering, Institute of Mechatronic Engineering, Chair of Machine Tools Development and Adaptive Controls, Technische Universität Dresden, Germany
[2] Fraunhofer Institute for Machine Tools and Forming Technology, Fraunhofer IWU, Germany
[*] E-mail: patrick.poehlmann@tu-dresden.de
https://doi.org/10.36897/jme/149902

are reduced. One way to overcome this issue is the implementation of control systems, which consider the physical interaction between the different drives. For example, in [3] a control strategy for a gantry stage, based on modal decoupling is presented. However, such systems require central data processing and are mostly not used in industry.

An alternative way to reduce bandwidth limitations is the integration of joints to create an additional DOF and to decrease the drives' mechanical coupling. For this purpose, compliant joints, which consist of a single deformable part, are preferable because of the low friction and backlash [4]. The previous work [5] shows that this strategy improves the bandwidth of the axis. Design of high precision motion systems with compliant elements is often addressed in literature. For example, in [6] a planar positioning system based on piezoelectric actuators is developed to provide a precise and frictionless motion. [7] describes the concept of a highly dynamic and lightweight machine structure, which is equipped with multiple feed drives and compliant mechanisms to decouple the drives and the guiding systems of each axis. In [8] KIM presents the design of joints for a gantry stage, which consist of a rotationally symmetrical arrangement of flexible links. The additional DOFs obtained by the concepts of [7] and [8] can be used to correct angular deviations of the machine.

This paper presents the design concept of compliant joints for a gantry type motion stage, to improve its positioning accuracy. First, a planar model of a gantry system is described in Section 2. This model is used to analyse the effect of remote pivot positions on the system's kinematic characteristics. Section 3 presents the design concept of compliant elements to optimise the stiffness characteristics of the complete joint. It is shown that using flexible links which consist of multiple layers of thin steel sheets is beneficial compared to one monolithic block. The experimental set-up, which is a two axis motion system driven by three linear motors, is introduced in Section 4. Four different configurations with varying pivot positions are examined in this investigation. Finally, Section 5 presents experimental findings on the rotational accuracy of the motion system.

2. KINEMATIC MODEL OF THE GANTRY STAGE

Figure 1 depicts a schematic model of the two-axis motion system consisting of rigid bodies for the drive units, the bridge plate and the X-slide as well as ideal rotational joints and linear guiding rails. The location of the pivots is defined by the distance between the joints d_G and the distance to the centre of the stage in Y-direction l_G. The position values x_1, x_2 and x_3 of the drives are used as inputs of the system. Applying a relative position to the drives of the Y-axis $x_\mathrm{rel} = x_1 - x_2$ results in a rotation of the stage about the Z-axis by the angle φ. The approximations $\sin(\varphi) \approx 0$ and $\cos(\varphi) \approx 1$ are used since only small angles φ are considered. The point C is located on the bridge plate in the centre between the two joint pivots and is calculated by:

$$\boldsymbol{r}_\mathrm{C} = \begin{pmatrix} x_\mathrm{C} \\ y_\mathrm{C} \\ \varphi_\mathrm{C} \end{pmatrix} = \begin{pmatrix} 0 & 0 \\ 1/2 & 1/2 \\ 1/d_\mathrm{G} & -1/d_\mathrm{G} \end{pmatrix} \begin{pmatrix} x_1 \\ x_2 \end{pmatrix} = \begin{pmatrix} 0 & 0 \\ 0 & 1 \\ 1/d_\mathrm{G} & 0 \end{pmatrix} \begin{pmatrix} x_\mathrm{rel} \\ x_\mathrm{lin} \end{pmatrix}, \tag{1}$$

where $x_{\mathrm{lin}} = x_1/2 + x_2/2$ is the mean position of the two drives and $x_{\mathrm{rel}} = x_1 - x_2$ is their difference in position. T, which is defined as the tool centre point (TCP), is located at the front of the X-slide with a distance l_{T} to the centre of the plate (Fig. 1). The position and orientation of T is given by:

$$\boldsymbol{r}_{\mathrm{T}} = \begin{pmatrix} x_{\mathrm{T}} \\ y_{\mathrm{T}} \\ \varphi_{\mathrm{T}} \end{pmatrix} = \begin{pmatrix} x_{\mathrm{C}} \\ y_{\mathrm{C}} \\ \varphi_{\mathrm{C}} \end{pmatrix} + \begin{pmatrix} x_3 - \varphi_{\mathrm{C}}(l_{\mathrm{T}} - l_{\mathrm{G}}) \\ l_{\mathrm{T}} + \varphi_{\mathrm{C}} x_3 \\ 0 \end{pmatrix}. \tag{2}$$

Inserting Eq. (1) into (2) and using $y_{\mathrm{C}} = (x_1 - x_2)/d_{\mathrm{G}}$ results in:

$$\boldsymbol{r}_{\mathrm{T}} = \begin{pmatrix} x_{\mathrm{T}} \\ y_{\mathrm{T}} \\ \varphi_{\mathrm{T}} \end{pmatrix} = \begin{pmatrix} (l_{\mathrm{G}} - l_{\mathrm{T}})/d_{\mathrm{G}} & -(l_{\mathrm{G}} - l_{\mathrm{T}})/d_{\mathrm{G}} \\ 1/2 + x_3/d_{\mathrm{G}} & 1/2 - x_3/d_{\mathrm{G}} \\ 1/d_{\mathrm{G}} & -1/d_{\mathrm{G}} \end{pmatrix} \begin{pmatrix} x_1 \\ x_2 \end{pmatrix} + \begin{pmatrix} x_3 \\ l_{\mathrm{T}} \\ 0 \end{pmatrix}. \tag{3}$$

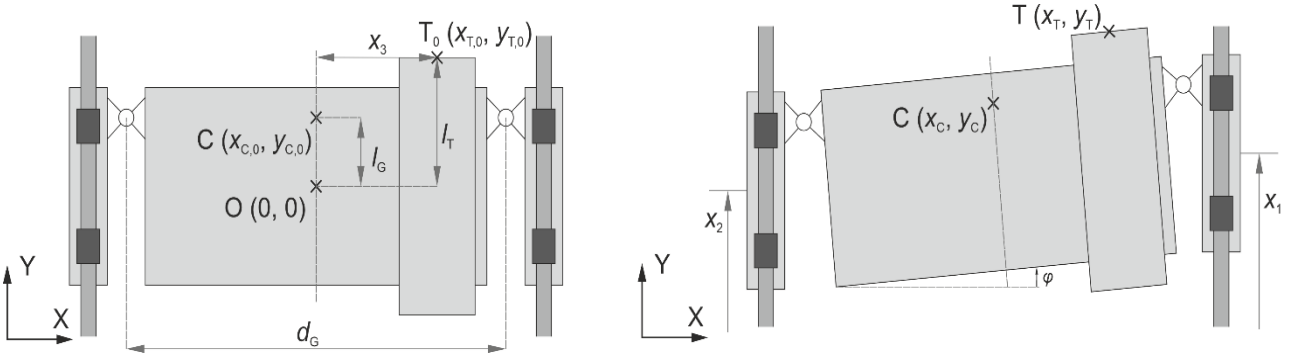

Fig. 1. Parametric model of the gantry stage with ideal joints

For further analysis, the system of equations (3) is linearised, considering an operating point, where the inputs are set to $x_1 = x_2 = x_{1,0}$ and $x_3 = x_{3,0}$.

$$\boldsymbol{r}_{\mathrm{T}} \approx \boldsymbol{r}_{\mathrm{T},0} + \Delta\boldsymbol{r}_{\mathrm{T}} = \boldsymbol{r}_{\mathrm{T},0} + \boldsymbol{J}\Delta\boldsymbol{x}, \tag{4}$$

where $\boldsymbol{r}_{\mathrm{T},0} = (x_{3,0} \quad x_{1,0} + l_{\mathrm{T}} \quad 0)^{\mathrm{T}}$. $\Delta\boldsymbol{r}_{\mathrm{T}}$ represents the vector of small displacements of T resulting from minor changes $\Delta\boldsymbol{x}$ of the input vector $\boldsymbol{x} = (x_1 \quad x_2 \quad x_3)^{\mathrm{T}}$, considering the transformation matrix $\boldsymbol{J}$:

$$\Delta\boldsymbol{r}_{\mathrm{T}} = \begin{pmatrix} \Delta x_{\mathrm{T}} \\ \Delta y_{\mathrm{T}} \\ \Delta\varphi_{\mathrm{T}} \end{pmatrix} = \underbrace{\begin{pmatrix} (l_{\mathrm{G}} - l_{\mathrm{T}})/d_{\mathrm{G}} & -(l_{\mathrm{G}} - l_{\mathrm{T}})/d_{\mathrm{G}} & 1 \\ 1/2 + x_{3,0}/d_{\mathrm{G}} & 1/2 - x_{3,0}/d_{\mathrm{G}} & 0 \\ 1/d_{\mathrm{G}} & -1/d_{\mathrm{G}} & 0 \end{pmatrix}}_{\boldsymbol{J}} \begin{pmatrix} \Delta x_1 \\ \Delta x_2 \\ \Delta x_3 \end{pmatrix}. \tag{5}$$

This equation is important for the accuracy at the TCP (T), because it describes the relationship between the vector of the smallest achievable displacements $\Delta\boldsymbol{r}_{\mathrm{T}}$ and the vector of the smallest position increments of the drives $\Delta\boldsymbol{x}$. To increase the accuracy at the TCP, the entries of the matrix $\boldsymbol{J}$, which are mainly influenced by the position of the joints,

need to be minimised. This is realised by maximising the distance of the joints d_G. By choosing l_G equal to l_T, two entries of $\boldsymbol{J}$ become equal to zero. This is preferable because in this case Δx_T depends only on the displacement of the third drive Δx_3. Thus, the motion in X-direction is decoupled from the remaining system. The relation between the force-torque vector $\boldsymbol{f}_\mathrm{T} = (f_\mathrm{x} \quad f_y \quad M)^\mathrm{T}$ at the point T and the corresponding drive forces is given by:

$$\begin{pmatrix} f_1 \\ f_2 \\ f_3 \end{pmatrix} = \underbrace{\begin{pmatrix} (l_\mathrm{G} - l_\mathrm{T})/d_\mathrm{G} & 1/2 + x_{3,0}/d_\mathrm{G} & 1/d_\mathrm{G} \\ -(l_\mathrm{G} - l_\mathrm{T})/d_\mathrm{G} & 1/2 - x_{3,0}/d_\mathrm{G} & -1/d_\mathrm{G} \\ 1 & 0 & 0 \end{pmatrix}}_{\boldsymbol{J}^\mathrm{T}} \begin{pmatrix} f_\mathrm{x} \\ f_y \\ M \end{pmatrix}. \tag{6}$$

Maximising d_G and choosing $l_\mathrm{G} = l_\mathrm{T}$ has a positive effect too, because it minimises the reaction forces on the drives. From this point of view, the system gets less sensitive to process loads $\boldsymbol{f}_\mathrm{T}$.

3. DESIGN OF THE COMPLIANT JOINTS

3.1. CONCEPT

The design of the compliant joints is based on the method of freedom and constraint topologies, described in [9]. The purpose is to link two bodies constraining their relative motion to a limited number of specific DOFs. All other DOFs are locked using a specific set of constraints. In the context of flexible links, one constraint can be seen as a straight line, which is characterised by a high reaction force on a coaxial deformation vector. Deformation vectors that are perpendicular to this axis result in a relatively small force value. Figure. 2a depicts an example of a simple joint with sheet elements, which are used as basic link elements in this investigation. Using at least two of these links leads to a single rotational DOF, if the angle α between the planes has a sufficient value.

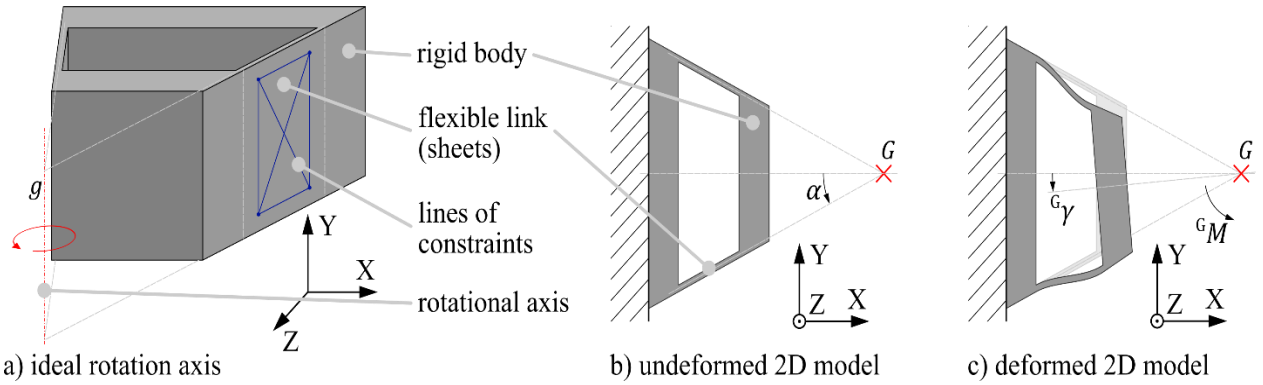

Fig. 2. Model of the compliant joint concept

The simplified two dimensional (2D) model of this arrangement is depicted in Fig. 2b. This representation considers only translation and rotation in the XY-plane, while other DOFs are neglected. The point G, where the extended axis of the links intersect, is called the geometric centre and can approximately be assumed as the pivot of the joint. The reaction force ${}^{\mathrm{G}}\boldsymbol{f}$ at the point G to its displacement ${}^{\mathrm{G}}\boldsymbol{u}$ is given by:

$$\underbrace{\begin{pmatrix} {}^{\mathrm{G}}f_x \\ {}^{\mathrm{G}}f_y \\ {}^{\mathrm{G}}M \end{pmatrix}}_{{}^{\mathrm{G}}\boldsymbol{f}} = \underbrace{\left(\begin{array}{cc|c} {}^{\mathrm{G}}k_{\mathrm{x}} & {}^{\mathrm{G}}k_{\mathrm{xy}} & {}^{\mathrm{G}}k_{\mathrm{x}\gamma} \\ {}^{\mathrm{G}}k_{\mathrm{yx}} & {}^{\mathrm{G}}k_{\mathrm{y}} & {}^{\mathrm{G}}k_{\mathrm{y}\gamma} \\ \hline {}^{\mathrm{G}}k_{\gamma\mathrm{x}} & {}^{\mathrm{G}}k_{\gamma\mathrm{y}} & {}^{\mathrm{G}}k_{\gamma} \end{array}\right)}_{{}^{\mathrm{G}}\boldsymbol{K}} \underbrace{\begin{pmatrix} {}^{\mathrm{G}}u_{\mathrm{x}} \\ {}^{\mathrm{G}}u_{\mathrm{y}} \\ {}^{\mathrm{G}}\gamma \end{pmatrix}}_{{}^{\mathrm{G}}\boldsymbol{u}}, \tag{7}$$

where ${}^{\mathrm{G}}\boldsymbol{K}$ is the stiffness matrix of the joint, which can be divided into four blocks. An ideal joint is obtained, if the linear deformations ${}^{\mathrm{G}}u_{\mathrm{x}}$ and ${}^{\mathrm{G}}u_{\mathrm{y}}$ are blocked and only a rotation ${}^{\mathrm{G}}\gamma$ is possible for any load ${}^{\mathrm{G}}\boldsymbol{f}$. This is not completely given, since the reaction force to a displacement is limited due to the compliance of the material. To maximise reaction forces to linear deformations ${}^{\mathrm{G}}u_{\mathrm{x}}$ and ${}^{\mathrm{G}}u_{\mathrm{y}}$, the upper left 2×2-matrix block is needed to have full rank and high values. Furthermore, the rotational stiffness ${}^{\mathrm{G}}k_{\gamma}$ is desired to be small. To minimise the cross coupling between rotational and linear deformation, the off-diagonal blocks need to be small as well. Ciblak [10] gives a good overview according to the problem of the elastic centre, which is a point where the off diagonal blocks vanish.

An essential concept used for the design of the joints is the division of the flexible links into multiple thin layers to adapt its stiffness properties. The following section analyses the effect of this method on the planar stiffness matrix of the link.

3.2. STIFFNESS OF PACKAGED LINK ELEMENTS

In the XY-plane, each flexible link is considered as a beam element with the modulus of elasticity E, the length L, the cross-section area A and the second moment of area I (see Fig. 3a). In this model, the beam connects the fixed ground on the left side to a rigid body on the right side. Applying a load vector ${}^{\mathrm{S}}\boldsymbol{f}$ to the point S of the rigid body leads to its displacement and rotation by the vector ${}^{\mathrm{S}}\boldsymbol{u}$ and to the deformation of the beam as illustrated in Fig. 3b. If the point S is located at the centre of the undeformed beam, the relationship between ${}^{\mathrm{S}}\boldsymbol{f}$ and small displacements ${}^{\mathrm{S}}\boldsymbol{u}$ is given by

$${}^{\mathrm{S}}\boldsymbol{f} = \begin{pmatrix} {}^{\mathrm{S}}f_x \\ {}^{\mathrm{S}}f_y \\ {}^{\mathrm{S}}M \end{pmatrix} = \underbrace{\begin{pmatrix} k_{\mathrm{x}} & 0 & 0 \\ 0 & k_{\mathrm{y}} & 0 \\ 0 & 0 & k_{\gamma} \end{pmatrix}}_{{}^{\mathrm{S}}\boldsymbol{K}} \underbrace{\begin{pmatrix} {}^{\mathrm{S}}u_{\mathrm{x}} \\ {}^{\mathrm{S}}u_{\mathrm{y}} \\ {}^{\mathrm{S}}\gamma \end{pmatrix}}_{{}^{\mathrm{S}}\boldsymbol{u}}, \tag{8}$$

where ${}^{\mathrm{S}}\boldsymbol{K}$ is the stiffness matrix of the beam at the point S. In this configuration, ${}^{\mathrm{S}}\boldsymbol{K}$ consists of the three main diagonal entries k_{x}, k_{y} and k_{γ}. Shear deformation is considered using the value Φ and the shear modulus G.

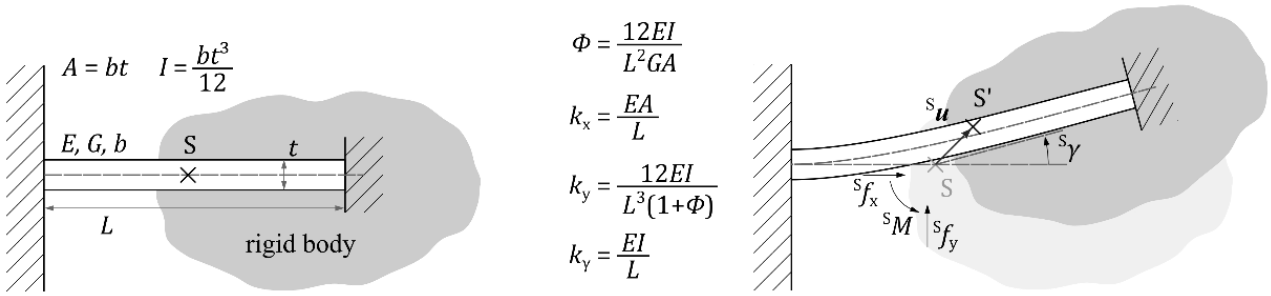

Fig. 3. Analytic model of a single beam element

In a package of N layers of beam elements (e), as depicted in Fig. 4a, each beam has a different distance Δy_i to the centre axis of the package. The transformation of the displacement vector ${}^{\mathrm{S}}\boldsymbol{u}_i$ and the force vector ${}^{\mathrm{S}}\boldsymbol{f}_i$ to an arbitrary point G (see Fig. 4b) on the axis of the package is calculated with the transformation ${}^{\mathrm{GS}}\boldsymbol{X}_i$:

$$ {}^{\mathrm{G}}\boldsymbol{u} = {}^{\mathrm{GS}}\boldsymbol{X}_i \cdot {}^{\mathrm{S}}\boldsymbol{u}_i, \;\; {}^{\mathrm{S}}\boldsymbol{f}_i = {}^{\mathrm{GS}}\boldsymbol{X}_i^{\mathrm{T}} \cdot {}^{\mathrm{G}}\boldsymbol{f}_i, \text{ with } {}^{\mathrm{GS}}\boldsymbol{X}_i = \begin{pmatrix} 1 & 0 & -\Delta y_i \\ 0 & 1 & \Delta x \\ -\Delta y_i & \Delta x & 1 \end{pmatrix}. \tag{9} $$

Using ${}^{\mathrm{GS}}\boldsymbol{X}_i$, the stiffness matrix ${}^{\mathrm{G}}\boldsymbol{K}^i$ of the i-th beam element corresponding to the point G is obtained:

$$ {}^{\mathrm{G}}\boldsymbol{K}^i = {}^{\mathrm{GS}}\boldsymbol{X}_i^{\mathrm{T}} \cdot {}^{\mathrm{S}}\boldsymbol{K}^{\mathrm{e}} \cdot {}^{\mathrm{GS}}\boldsymbol{X}_i = \begin{pmatrix} k_{\mathrm{x}}^{\mathrm{e}} & 0 & -\Delta y k_{\mathrm{x}}^{\mathrm{e}} \\ 0 & k_{\mathrm{y}}^{\mathrm{e}} & \Delta x k_{\mathrm{y}}^{\mathrm{e}} \\ -\Delta y k_{\mathrm{x}}^{\mathrm{e}} & \Delta x k_{\mathrm{y}}^{\mathrm{e}} & \Delta y_i^2 k_{\mathrm{x}}^{\mathrm{e}} + \Delta x_i^2 k_{\mathrm{y}}^{\mathrm{e}} + k_{\gamma}^{\mathrm{e}} \end{pmatrix} \tag{10} $$

The full stiffness matrix of the package ${}^{\mathrm{G}}\boldsymbol{K}^{\Sigma}$ is calculated from the sum of all N elements:

$$ {}^{\mathrm{G}}\boldsymbol{K}^{\Sigma} = \sum_{i=1}^{N} {}^{\mathrm{G}}\boldsymbol{K}^i = \begin{pmatrix} N k_{\mathrm{x}}^{\mathrm{e}} & 0 & 0 \\ 0 & N k_{\mathrm{y}}^{\mathrm{e}} & N\Delta x k_{\mathrm{y}}^{\mathrm{e}} \\ 0 & N\Delta x k_{\mathrm{y}}^{\mathrm{e}} & N\Delta x^2 k_{\mathrm{y}}^{\mathrm{e}} + N^3 k_{\gamma}^{\mathrm{e}} \end{pmatrix}. \tag{11} $$

If the full package from Fig. 4 is substituted by one monolithic (M) beam, the stiffness matrix corresponding to the point G is given by:

$$ {}^{\mathrm{G}}\boldsymbol{K}^{\mathrm{M}} = \begin{pmatrix} k_{\mathrm{x}}^{\mathrm{M}} & 0 & 0 \\ 0 & k_{\mathrm{y}}^{\mathrm{M}} & k_{\mathrm{y}}^{\mathrm{M}} \\ 0 & \Delta x k_{\mathrm{y}}^{\mathrm{M}} & \Delta x^2 k_{\mathrm{y}}^{\mathrm{M}} + k_{\gamma}^{\mathrm{M}} \end{pmatrix} = \begin{pmatrix} {}^{\mathrm{G}}k_{\mathrm{x}}^{\mathrm{M}} & 0 & 0 \\ 0 & {}^{\mathrm{G}}k_{\mathrm{y}}^{\mathrm{M}} & {}^{\mathrm{G}}k_{\mathrm{y}\gamma}^{\mathrm{M}} \\ 0 & {}^{\mathrm{G}}k_{\mathrm{y}\gamma}^{\mathrm{M}} & {}^{\mathrm{G}}k_{\gamma}^{\mathrm{M}} \end{pmatrix}. \tag{12} $$

According to the relation between the cross-section of a single element e and the monolithic block M ($A^{\mathrm{M}} = NA^{\mathrm{e}}$ and $I^{\mathrm{M}} = N^3 I^{\mathrm{e}}$), ${}^{\mathrm{G}}\boldsymbol{K}^{\Sigma}$ can be represented by the stiffness components $k_{\mathrm{x}}^{\mathrm{M}}$, $k_{\mathrm{y}}^{\mathrm{M}}$ and k_{γ}^{M} of the monolithic link:

$$ {}^{\mathrm{G}}\boldsymbol{K}^{\Sigma} = \begin{pmatrix} k_{\mathrm{x}}^{\mathrm{M}} & 0 & 0 \\ 0 & k_{\mathrm{y}}^{\mathrm{M}}/N^2 & \Delta x k_{\mathrm{y}}^{\mathrm{M}}/N^2 \\ 0 & \Delta x k_{\mathrm{y}}^{\mathrm{M}}/N^2 & \Delta x^2 k_{\mathrm{y}}^{\mathrm{M}}/N^2 + k_{\gamma}^{\mathrm{M}} \end{pmatrix} = \begin{pmatrix} {}^{\mathrm{G}}k_{\mathrm{x}} & 0 & 0 \\ 0 & {}^{\mathrm{G}}k_{\mathrm{y}}^{\Sigma} & {}^{\mathrm{G}}k_{\mathrm{y}\gamma}^{\Sigma} \\ 0 & {}^{\mathrm{G}}k_{\mathrm{y}\gamma}^{\Sigma} & {}^{\mathrm{G}}k_{\gamma}^{\Sigma} \end{pmatrix}. \tag{13} $$

Comparing ${}^{\mathrm{G}}\boldsymbol{K}^{\Sigma}$ and ${}^{\mathrm{G}}\boldsymbol{K}^{\mathrm{M}}$ one finds that the number of the elements N significantly reduces the stiffness values of the lower right 2×2-block in Eq. (13). In particular, it is advantageous to keep the value of the rotational stiffness ${}^{\mathrm{G}}k_{\gamma}^{\Sigma}$ small when G is assumed to be the desired rotational centre of the joint.

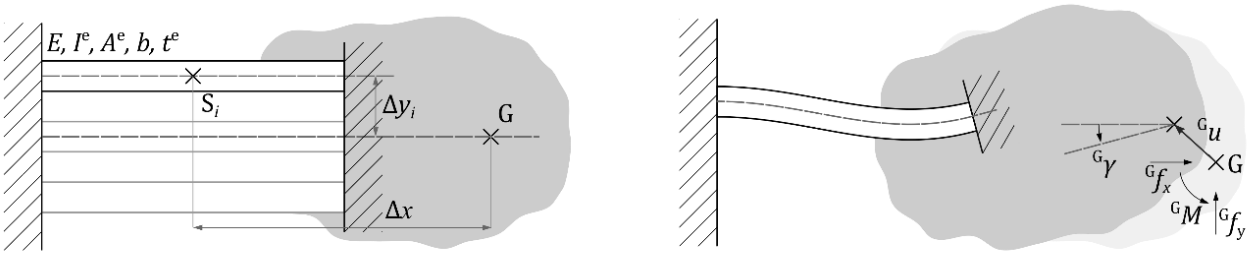

a) Package of flexible link elements b) Deformation of one link element

Fig. 4. Model of single beam in a packaged link

To obtain the configuration depicted in Fig. 2 the flexible link needs to be rotated to its final orientation. Considering the transformation matrix of the i-th link the full stiffness matrix of the joint ${}^{\mathrm{G}}\boldsymbol{K}$ is given by the sum of the stiffness matrices ${}^{\mathrm{G}}\boldsymbol{K}^{i}$ of all links:

$$\boldsymbol{R}_i = \begin{pmatrix} c_i & -s_i & 0 \\ s_i & c_i & 0 \\ 0 & 0 & 1 \end{pmatrix}, \text{where } c_i = \cos(\alpha_i) \text{ and } s_i = \sin(\alpha_i), \tag{14}$$

$${}^{\mathrm{G}}\boldsymbol{K}^{i} = \boldsymbol{R}_i^{\mathrm{T}} \cdot {}^{\mathrm{G}}\boldsymbol{K}^{\mathrm{L}i} \cdot \boldsymbol{R}_i = \begin{pmatrix} c_i^2\,{}^{\mathrm{G}}k_{\mathrm{x}}^{\mathrm{L}} + s_i^2\,{}^{\mathrm{G}}k_{\mathrm{y}}^{\mathrm{L}} & s_i c_i({}^{\mathrm{G}}k_{\mathrm{x}} - {}^{\mathrm{G}}k_{\mathrm{y}}^{\mathrm{L}}) & -s_i\,{}^{\mathrm{G}}k_{\mathrm{y}\gamma}^{\mathrm{L}} \\ s_i c_i({}^{\mathrm{G}}k_{\mathrm{x}}^{\mathrm{L}} - {}^{\mathrm{G}}k_{\mathrm{y}}^{\mathrm{L}}) & s_i^2\,{}^{\mathrm{G}}k_{\mathrm{x}}^{\mathrm{L}} + c_i^2\,{}^{\mathrm{G}}k_{\mathrm{y}}^{\mathrm{L}} & c_i\,{}^{\mathrm{G}}k_{\mathrm{y}\gamma}^{\mathrm{L}} \\ -s_i\,{}^{\mathrm{G}}k_{\mathrm{y}\gamma}^{\mathrm{L}} & c_i\,{}^{\mathrm{G}}k_{\mathrm{y}\gamma}^{\mathrm{L}} & {}^{\mathrm{G}}k_{\gamma}^{\mathrm{L}} \end{pmatrix}, \tag{15}$$

where the link L can either be a package (Σ) or a monolithic block (M). Considering the requirements from Section 3.1, the minimising of ${}^{\mathrm{G}}k_{\mathrm{y}\gamma}^{\mathrm{L}}$ and ${}^{\mathrm{G}}k_{\gamma}^{\mathrm{L}}$ is important to diminish the off-diagonal blocks of ${}^{\mathrm{G}}\boldsymbol{K}$ in Eq. (7) as well as the reaction torque ${}^{\mathrm{G}}M$ caused by a rotational displacement ${}^{\mathrm{G}}\gamma$. ${}^{\mathrm{G}}k_{\mathrm{y}}^{\mathrm{L}}$ has a small value compared to ${}^{\mathrm{G}}k_{\mathrm{x}}^{\mathrm{L}}$, particularly if the packaged link is used. High stiffness components to linear displacements (upper left block) are achieved by combining at least two links with different angles α_i, where each link ensures a high stiffness in its longitudinal axis.

4. EXPERIMENTAL CONFIGURATION

4.1. GANTRY STAGE

The investigation focuses a gantry-type motion stage equipped with two linear motors f_1 and f_2 (Tecnotion UXX6N) and optical measurement systems (Heidenhain LIC4117) with an accuracy of ± 5 µm and a resolution of 1 nm (see Fig. 5a). Two linear rails with a distance

of 770 mm guide the two drive units (two carriages each). The second axis x_3 consists of a linear motor (Tecnotion UM6N) and an optical measurement system (Numeric Jena LAK11, accuracy: ±3 µm, resolution: 10 nm). With a load mass of about 12.3 kg (X-slide), the complete gantry stage has a weight of about 45 kg. A PC-based real-time control system (TwinCAT3 by Beckhoff) is used to generate motion trajectories, while each drive's cascaded position-velocity-current-control (P-PI-PI) is implemented within the servodrive (Beckhoff AX5206 for the Y-axis and AX5103 for the X-axis).

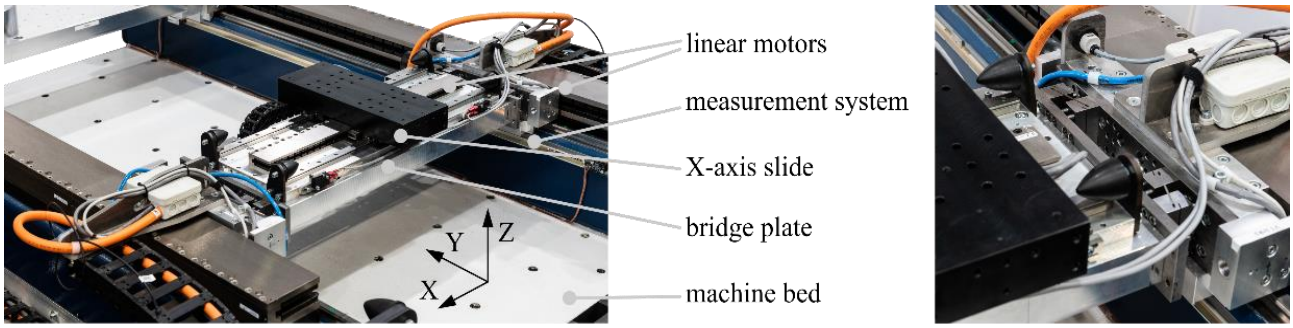

a) Two axis motion system (gantry stage) b) Modular coupling elements (configuration 1a)

Fig. 5. Full configuration of the experimental set-up

Exchangeable coupling elements connect the aluminium bridge plate to the drive units on each side (Fig. 5b). These elements are designed to work as rotational joints using flexible links (see Section 3).

4.2. JOINT CONFIGURATIONS

Figure 6 illustrates the arrangement of the two compliant joints, that are the subject of this investigation. Each of them consists of two flexible links as well as two connection plates to mount the joints between the bridge plate and the drive unit of the gantry stage. The links are composed of spring steel sheets and act as beam elements in the X-Y-plane with a high stiffness corresponding to their longitudinal direction. Depending on the arrangement of the links, the pivot G can be placed outside of the joint (remote centre). [5] presents a joint configuration, where the pivot is located in its centre. However, the exact centre of the rotation depends on the arrangement of the links, their stiffness matrices as well as the load conditions (see e.g. [10]). Each flexible link itself consists of multiple layers of thin sheets to decrease its stiffness to deformations in the normal direction of its plane. As shown in Section 3.2, this method reduces the rotational stiffness of the joints. In [5], the reduction of the full system's rotational stiffness is shown using measured frequency response functions.

Figure 7 depicts the four configurations of the gantry stage, which were realised with the two joint arrangements shown in Fig. 6. The most significant difference between them is the position of the geometric centres of the joints in the XY-plane. The design properties of the flexible links are listed in Table 1.

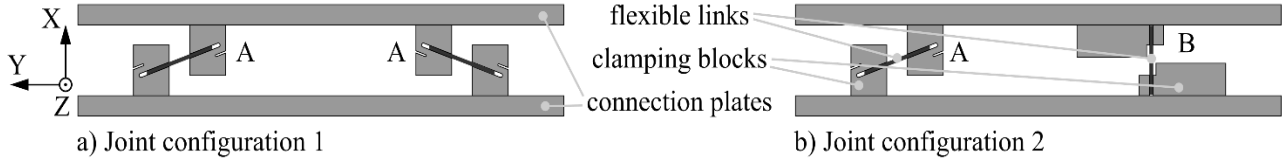

a) Joint configuration 1 b) Joint configuration 2

Fig. 6. Layout of the joint elements

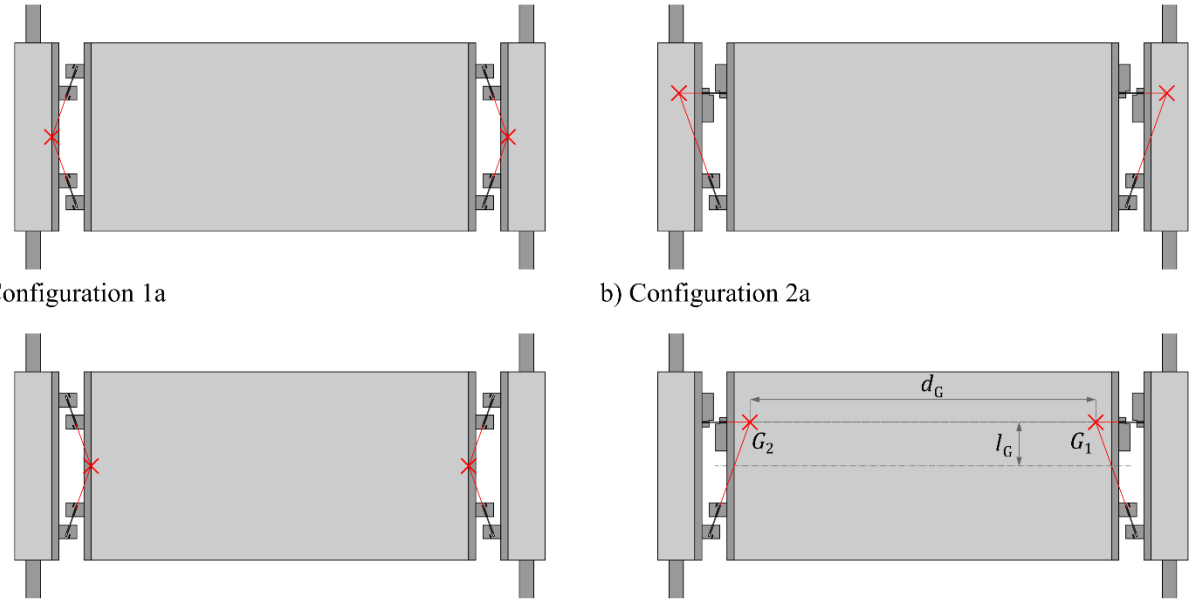

a) Configuration 1a b) Configuration 2a

c) Configuration 1b d) Configuration 2b

Fig. 7. Gantry stage configurations with compliant joints

Table 1. Design parameters of the joint configurations

Configuration	Flexible link	Number of steel sheets	Thickness per sheet (mm)	Free length (mm)	Geometric joint position d_G (mm)	Geometric joint position l_G (mm)
1a	A	8	0.2	11.7	709.6	0.0
	A	8	0.2	11.7		
1b	A	8	0.2	11.7	600.4	0.0
	A	8	0.2	11.7		
2a	B	8	0.2	25.0	753.2	60.0
	A	8	0.2	11.7		
2b	B	8	0.2	25.0	556.8	60.0
	A	8	0.2	11.7		

5. EXPERIMENTAL INVESTIGATIONS

In this section, the capability to correct the angular deviation of the motion system equipped with the compliant joints is analysed. For this purpose, the effective value of the distance of the pivot d_G is determined for each configuration. All measurements, which are described in the following sections, are accomplished using the API XD Laser measuring system with an angular accuracy of about ±15 µrad in the experiments.

5.1. JOINT DISTANCE

In order to identify the effective distance between the two pivots d_G of the experimental arrangement, the relationship between the difference of the Y-axis x_rel (see Eq. (1)) and the actual angle φ of the X-slide (derived from the laser-measurement) is determined. Figure 8a shows the reference trajectories of the two drives with a maximum difference of $x_\mathrm{rel} = 0.8$ mm. The trajectories are divided in small steps of $\Delta x_\mathrm{rel} = 0.05$ mm. After reaching the reference position of each step, the position is held for four seconds and multiple measurements are taken with an interval of 0.1 s. The full motion profile is repeated three times. Considering the equation:

$$\varphi_i = p_1 \cdot x_{\mathrm{rel},i} + p_0 + e_i, \tag{16}$$

of the ith measurement, the parameters p_0 and p_1 are determined by minimising the error e_i with least squares regression. The error of the regression is depicted in Fig. 8b for all configurations. With the gradient $p_1 = \Delta\varphi/\Delta x_\mathrm{rel}$ the distance d_G is estimated:

$$\overline{d_G} = 1/p_1. \tag{17}$$

The offset value p_0 results from the mounting conditions of the laser measuring system and is not considered in further investigations. Table 2 lists the resulting values of $\overline{p_1}$ and $\overline{d_G}$. The identified values $\overline{d_G}$ differ from the geometric design parameters d_G within a range of up to 1 %. Reasons for this are the compliance of other components of the motion stage and, in particular, the mounting conditions of the joints themselves. However, all configurations show linear behaviour and small angular errors to the regression line (Fig. 8b). The conclusion is that if the exact distance $\overline{d_G}$ is identified, the angle of the stage can be set precisely. Comparing the resulting mean errors of the regression, configurations with a smaller $\overline{d_G}$ show greater errors. Furthermore, the configurations 1a and 1b are more accurate than the configurations 2a and 2b.

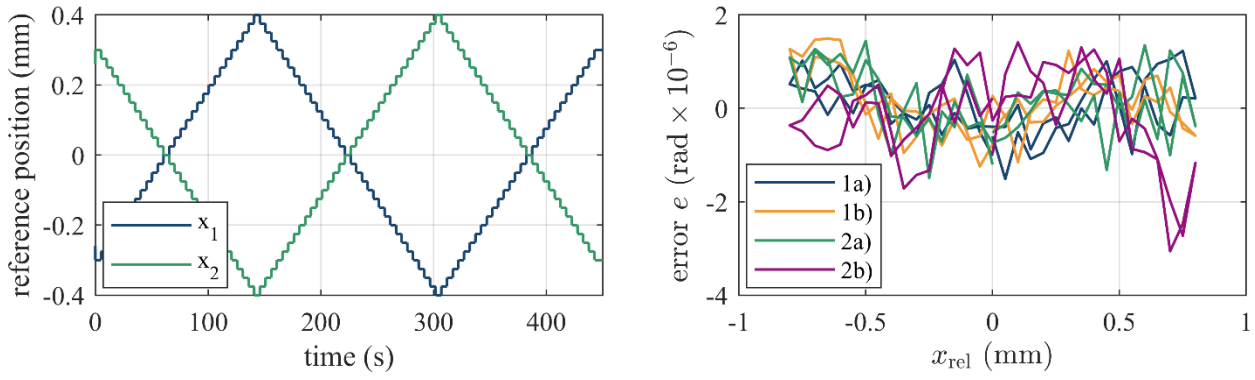

a) Y-axis position x_1 and x_2 b) regression error

Fig. 8. Linear regression

Table 2. Parameters of the linear regression

Configuration	Gradient p_1 (rad/m)	$\varphi_{\max}$ (10^{-3} rad)	Mean error (10^{-6} rad)	$\overline{d_G}$ (mm)	$\frac{\overline{d_G} - d_G}{d_G}$ (%)
1a	1.397	1.12	0.477	715.8	0.87
1b	1.673	1.34	0.646	597.6	–0.47
2a	1.316	1.05	0.643	760.1	0.92
2b	1.807	1.45	0.816	553.5	–0.59

5.2. ANGULAR CORRECTION

Geometric inaccuracies of the individual components, as well as mounting conditions, lead to positioning errors of the motion stage. In the first step of this experiment, the angle φ is measured as a function of the Y-axis position with $x_{\text{rel}} = 0$. The measured angular deviations φ_{meas} are inherent to the axis configuration due to the limited parallelism of the linear guiding rails and their straightness errors. To show the effectiveness of the compliant joints in a practical application, a table of correction values x_1 and x_2 for the angle φ_{meas} is generated and applied to the two drives of the Y-axis in the second step. The measurement is conducted with the laser system in a position range of 640 mm with an interval of 20 mm and is repeated three times in both directions. Figure 9a depicts the resulting angle φ (free of average values).

The table of correction values is calculated using the mean values of the measured angle at each position (both directions), considering the identified gradient p_1. The list of displacement values is divided by two and applied to both Y-axes drives in opposite directions. This procedure is carried out for each of the joint configurations 1b), 2a) and 2b) independently.

The results of the measurement after the corrections are shown in Fig. 9b. Compared to the measurement without correction, the angular variance is reduced significantly for all configurations. The remaining error is characterised by the difference between the positive and negative direction of the motion, in particular for configuration 2a and 2b. A conceivable reason for this is the arrangement of the links in these configurations. The links on the left and right joint are on the same axis. This leads to a bistable behaviour due to inaccuracies of the distance between the guiding rails.

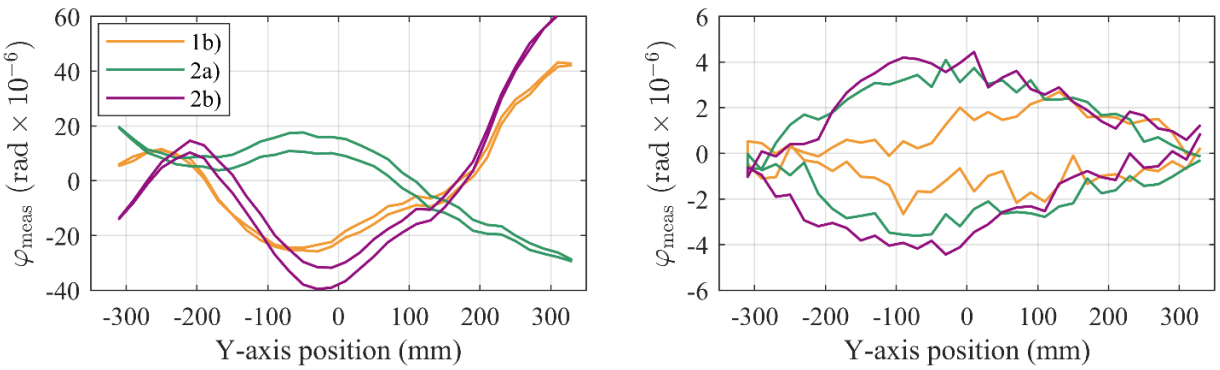

a) Without angular correction b) With angular correction

Fig. 9. Angular error of the Y-axis

6. CONCLUSION

This contribution presents a design concept of compliant joints to improve the accurracy of a gantry-type motion system. The flexible links consist of a package of multiple thin steel sheets, instead of a monolithic component, to adjust its stiffness characteristics and to reduce the rotational stiffness of the complete joint. The position of the joint's pivot can even be placed outside the joint by the arrangement of the links. If equipped with these joints, the kinematic characteristics of the gantry stage can be adapted. It is possible to decouple the X- and Y-axis' motion of the TCP and to increase the angular accuracy. Another benefit of the joints is the reduction of the reaction forces on the drives and also on the guidings when correcting angular errors. Modular designed joint elements are developed to analyse different configurations of the flexible joint. Experiments demonstrate a high angular accuracy if the effective distance of the pivots is known. The measurement of reaction forces for the gantry stage with and without flexible joints is the subject of future work.

ACKNOWLEDGEMENTS

This research was supported by a German Research Foundation (DFG) grant, received within the research project 'Application potential of articulated coupled drive and guide elements for increase of movement dynamics and accuracy' (269296582), which is gratefully acknowledged.

REFERENCES

[1] HIRAMOTO K., HANSEL A., DING S., YAMAZAKI K., 2005, *A Study on the Drive at Center of Gravity (DCG) Feed Principle and Its Application for Development of High Performance Machine Tool Systems*, CIRP Annals, 45/1, 333–336.

[2] PEUKERT C., MERX M., MÜLLER J., IHLENFELDT S., 2017, *Flexible Coupling of Drive and Guide Elements for Parallel-Driven Feed Axes to Increase Dynamics and Accuracy of Motion*, Journal of Machine Engineering, 17/2, 77–89.

[3] HARCIA-HERREROS I., HESTELYN X., GOMAND J., COLEMAN R., BARRE P., 2013, *Model-Based Decoupling Control Method for Dual-Drive Gantry Stages: A Case Study with Experimental Validations*, Control Engineering Practice, 21/3, 298–307.

[4] HOWELL L.L., MAGLEBY S.P., OLSEN B.M., 2013, *Handbook of Compliant Mechanisms*, John Wiley & Sons, Chichester.

[5] PÖHLMANN P., PEUKERT C., MERX M., MÜLLER J., IHLENFELDT S., 2020, *Compliant Joints for the Improvement of the Dynamic Behaviour of a Gantry Stage with Direct Drives*, Journal of Machine Engineering, 20/3, 17–29.

[6] ELFIZY A.T., BONE G.M., ELBESTAWI M.A., 2005, *Design and Control of a Dual-Stage Feed Drive*, International Journal of Machine Tools and Manufacture, 45/2, 153–165.

[7] IHLENFELDT S., MÜLLER J., MERX M., PEUKERT C., 2018, *A Novel Concept for Highly Dynamic Over-Actuated Lightweight Machine Tools*, Reinventing Mechatronics: Proceedings of Mechatronics, 210–216.

[8] KIM K., AHN D., GWEON D., 2012, *Optimal Design of a 1-Rotational DOF Flexure Joint for a 3-DOF H-Type Stage*, Mechatronics, 22/1, 24–32.

[9] HOPKINS J.B., CULPEPPER M.L., 2010, *Synthesis of Multi-Degree of Freedom, Parallel Flexure System Concepts via Freedom and Constraint Topology (FACT) – Part I: Principles*, Precision Engineering, 34/2, 259–270.

[10] CIBLAK N., LIPKIN H., 2003, *Design and Analysis of Remote Center of Compliance Structures*, Journal of Robotic Systems, 20/8, 415–427.